Food Control 121 (2021) 107638

Contents lists available at ScienceDirect

Food Control

journal homepage: www.elsevier.com/locate/foodcont

Non-destructive control in cheese processing: Modelling texture evolution in the milk curdling phase by laser backscattering imaging

Samuel Verdú [a,*], Alberto J. Pérez [b], José M. Barat [a], Raúl Grau [a]

[a] Departamento de Tecnología de Alimentos. Universidad Politècnica de València, Spain
[b] Departamento de Informática de Sistemas y Computadores, Universidad Politècnica de València, Spain

ARTICLE INFO

Keywords:
Cheese production
Laser backscattering imaging
Non-destructive control
Curdling process
Monitoring
Prediction
Phase change

ABSTRACT

This study aim was to explore the laser backscattering imaging technique's capacity to model the curdling phase in cheese processing. To do so, three different formulas were studied by modifying solute concentration. Textural modifications to the matrix during curdling were characterised by viscosimetry and texture measurements depending on samples' liquid or solid state. This state changed by determining gelation to establish the limits for the liquid and solid phases. The process was also characterised by the imaging technique, which showed dependence on both solute concentration and enzymatic effect on both the previously observed phases. After following multivariate statistical procedures to reduce dimensionality, the imaging results revealed that solute concentration strongly influenced the variance that the imaging technique captured. It reduced the visibility of the phase change in the image parameters. After eliminating this influence, the evolution of the matrix across the liquid and solid phases was modelled. Data were divided into phases and used to successfully predict the matrix status in each phase by multivariate non-linear regression procedures. It was concluded that the laser backscattering imaging technique presented suitable properties to be used for non-destructive continuous curdling process monitoring during the cheese-making process.

1. Introduction

One of the most important stages in the cheese-making process is curdling (Everard et al., 2007). The main objective of this phase is to pass the milk matrix from a liquid state to a solid state by progressive gelation. This can be done in two ways: adding enzymes (chymosin) that modify casein structures by reducing solubility; lowering pH, raising the isoelectric point of proteins and then reducing solubility. Casein represents around 80% of the protein fraction of milk that forms part of the milk matrix as dispersed clusters known as micelles. These clusters are assumed to be spherical structures formed by different protein subunits (α_{s1}, α_{s2}, β and κ-casein), calcium and phosphate (Harton & Shimizu, 2019). The distribution of the distinct caseins is heterogenic throughout this structure. Indeed κ-caseins play a crucial role in the process because of their hydrophilic nature. It is located principally on the micelle surface from where it stabilises structures and prevents them from aggregating (Vacca et al., 2020). So the enzymatic activity that takes place in the curdling phase involves modifying the hydrophilic properties of casein micelles. Such modifications focus on the surface via the proteolysis of the Phe_{105}-Met_{106} bonds of κ-casein, which then induces aggregation and three-dimensional space-filling gel formation. The curdling process comprises two phases after enzyme addition: proteolysis and aggregation (Bittante et al., 2012). However, it is difficult to control phases because aggregation overlaps the proteolysis reaction; the latter is certainly not complete before aggregation begins. Aggregation forms increasingly bigger structures until the matrix eventually acquires the solid nature of gel. From this point, the matrix components and enzymes retained in structural spaces diminish movement capacity, but continue working until gel maturation ends.

The kinetics of this enzymatic process involve many factors that directly affect the end product's physico-chemical properties, and then its quality features. Some include the origin of milk, enzyme concentration, solute concentration, temperature, presence of calcium, etc. (Panthi et al., 2019). Any variation in these factors can affect the enzyme activity kinetics and then modify the formed curd's optimal cutting time. Alterations to cutting times may have certain effects, such as excess whey loss, increased gel hardness, large amounts of water accumulating, etc. Thus knowledge about the milk matrix status in the

* Corresponding author. Edificio 8E - Acceso F – Planta 0 Ciudad Politécnica de la Innovación, Universidad Politécnica de Valencia, Camino de Vera, s/n, 46022, Valencia, Spain.
E-mail address: saveram@upvnet.upv.es (S. Verdú).

https://doi.org/10.1016/j.foodcont.2020.107638
Received 1 July 2020; Received in revised form 15 September 2020; Accepted 16 September 2020
Available online 18 September 2020

curdling phase obtained by control techniques is fundamental for avoiding modifications being made to product properties due to variations in cutting times.

The control and characterisation of this process have been put into practice by different approaches through both continuous online monitoring and laboratory analysis applications. Most instrumental methods work via destructive procedures by measuring physical properties, such as viscosity and other textural parameters (Aldalur et al., 2019), which can bring about major alterations to the milk matrix. These devices also limit the development of other online applications on cheese production chains, such us curd-cutting applications (O'Callaghan et al., 2002). Several non-destructive applications have been developed for curdling process characterisation, which are based on different principles: ultrasound (Jiménez et al., 2017), optical techniques (Arango & Castillo, 2018; Castillo et al., 2005; Mateo et al., 2010), nuclear magnetic resonance (Curti et al., 2019) and different image analysis procedures (Darnay et al., 2017). With image analysis procedures, laser-backscattering imaging characterises the extinction of light transmittance across a changing magnitude measured in a given matrix. This principle has already been used to monitor the curdling process, but as a classic optical turbidimetry approach (Lomholt et al., 1998), which presents certain limitations like the need for a diluted milk sample. Laser-backscattering imaging follows this principle, but applies a more powerful light source, while imaging analysis and data mining techniques are followed to study the generated diffraction patterns because of milk matrix-light interactions. The possibilities of acquiring information from continuous processes increase with these features, which improve knowledge on the produced phenomena. This imaging technique has been applied to model different features in food processing and products, such as predicting textural properties of vegetable creams (Verdú et al., 2018), modelling the effect of fibre enrichment on biscuit properties (Verdú et al., 2019a) or characterising antimicrobial particles with essential oils (Verdú et al., 2020). Indeed the successful application to non-destructive yogurt fermentation modelling (Verdú et al., 2019b) prompted to work on applying this technique to control other production chains in the dairy industry. Moreover, cheese production involves operations with biochemical similarities and the fact that it is controlled by this technique is most interesting.

Thus the present work aimed to study the capacity of laser backscattering imaging to continuously control and model milk curdling phase kinetics in a non-destructive mode.

2. Material and methods

2.1. Sample preparation and the milk curdling process

The raw materials employed for curd formulas were fresh whole cow's milk (4.5 ± 0.3% carbohydrates, 3.1 ± 0.3% proteins, 3.5 ± 0.5% lipids) and skimmed milk powder (MP, 54 ± 1.5% carbohydrates, 33 ± 1.9% proteins, 1 ± 0.3% lipids), which were purchased from a local distributor. Animal rennet (chymosin 80% w/v, 180 international milk clotting units (IMCU)/mL) was supplied by the company Productos Nievi S.L. (Biscay, Spain). $CaCl_2$ was obtained from Sigma-Aldrich (Madrid-Spain).

Three different formulations based on several levels of dry matter were selected to test the imaging system in the studied matrix, and significant differences in curdling kinetics and textural terms appeared. For this purpose, modifications were made by amending the amount of added skimmed milk powder. Thus modifications to the dry matter concentration of the matrix led to alterations in the texture and curdling kinetics, which allowed to study the capacity of the designed device in order to model the process under different conditions in composition terms. Thus three different MP levels were added: 1%, 6% and 8% w/v (w.b). The procedure for all formulas was the same and is detailed below:

A volume of 150 mL of fresh whole milk was heated to 40 °C with stirring. Skimmed milk powder at the defined proportion and 0.15 g of $CaCl_2$ (0.001% w/v) were added until complete dissolution. A fraction of 100 mL of the mixture was divided into two thermoformed polystyrene cylindrical containers (7 cm high, 5.5 cm diameter). The first container was used for the viscosity/texture analysis, and the second one for the image analysis. This container was selected to simplify sample handling during the experiment, following previous experiences when modelling other dairy processes (Verdú et al., 2019b). The cylindrical shape and selected dimensions allowed a homogeneous heat transfer from the heat exchanger to the matrix, and also avoided container walls interacting with the laser beam during analyses.

The curdling process was started by adding two drops of rennet and manual mixing for 5 s. Then samples were left for 30 min at 40 °C to ensure the complete phase transition from milk to curd following the rennet provider's instructions. Temperature was maintained in both analysis systems by a tubular heat exchanger connected to an Ultraterm 200 thermostat (JP Selecta, Barcelona, Spain). The experiment was replicated 10 times per formula from 10 different milk batches.

2.2. Imaging device

To obtain continuous information from the milk curdling phase generated by the light-milk matrix interaction during the curdling process, a low-cost device was built consisting in a coherent light and a digital camera connected to a computer. Fig. 1-A shows the device setup. The elements of the curdling setup were a digital camera as a capture system, a laser pointer, a computer and a heat exchanger. The device was placed inside a dark cabin to keep it away from light. The capture system for the image analysis was a digital Logitech C920 camera with a CMOS sensor, which operates at a resolution of 2304 × 1535. The exposure and gain settings were configured to the auto mode. The camera included an HD video that worked in the H.264 high quality format. Images were obtained in the RGB (red, green and blue) format and were saved as.JPEG (dimension of 1980 × 1080). The camera was vertically placed 15 cm over the sample surface. The sample container was coupled to the heat exchanger in the middle of the vision field. The laser pointer (650 nm, 50 mW, 3 mmø) was perpendicularly placed 20 cm under the milk container by projecting on the central zone of the bottom surface. Both the laser diode and camera were connected to a conventional computer that ran Linux. The system was controlled by a specific program that automatically triggered the camera by software to take images at a rate of 1 image/sec. while the milk curdling process was underway (30 min). At the end of the curdling phase, 1800 images from each sample had been obtained. Ten samples per formula from 10 different milk batches were analysed.

2.3. Image processing and data collection

The images captured while monitoring the curdling process were the data reservoir from which the information on changes in the milk matrix-laser interactions was collected. The software was used to follow the data collection protocol. This software was based on a previous application, which is explained in Verdú et al. (2020). It was developed in the C language using OpenCV 2.4.1 image processing libraries (Bradski, 2000) to quickly and accurately process images. It ran on a computer with the Linux Ubuntu 16.04 operating system. The protocol was run as follows:

The first step was to generate an image-stack from the entire process. All the images were transformed into a greyscale (8 bits) to simplify the collected data. The 1800 images captured during the curdling process were joined to an image stack, where the Y-axis represented time. The result was a three-dimensional space of pixels, where variation in diffraction patterns was collected with time (Fig. 1-B). The second step was to extract the orthogonal images. The changes in light intensity that took place throughout the curdling process were captured in orthogonal images to simplify the monitoring process from 1800 images to 1 image.

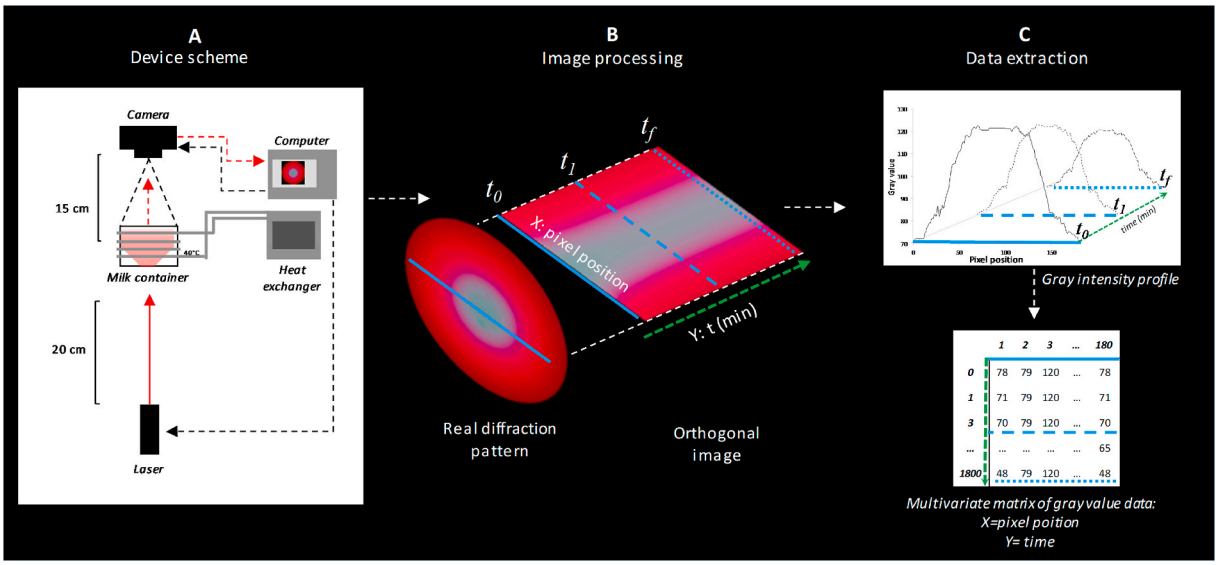

Fig. 1. Scheme of the device and data processing. Laser backscattering imaging device (A), image processing (B) and data extraction (C).

This one image was generated by slicing the stack across the time axis (Y). Slice size was 50 mm wide (diameter of the sample's container), which crossed the central zone of the captured diffraction pattern (Fig. 1-B, continuous blue line). This width corresponded to 180 pixels, which were assumed as single variables to collect variance in intensity themselves. The obtained image contained the intensity profile of the diffraction pattern along the X-axis at each time on the Y-axis. Hence each orthogonal image represented a data matrix of changes in intensity profiles with time. The last procedure was to collect intensity data from orthogonal images. Data were extracted as the grey values of each 180 variable (pixels) from the profile of the diffraction pattern (X-axis) for all 1800 time captures (pixels of the Y-axis). The whole extracted matrix was organised and labelled in a common data matrix to study not only the evolution of each variable with time, but also the relation with the curdling process status in textural terms later on (Fig. 1-C).

2.4. Texture analysis

Measuring milk mechanical properties during the curdling process is a complex task because of the modification of matrix status in physical state terms with time, which makes using a single method for either the fluid or the solid matrix difficult. Therefore in order to interpret the data collected by the imaging analysis throughout the process, two methods were used to obtain data from the textural status of the milk matrix depending on whether the state was liquid or solid. In the liquid phase, a rotational viscosimeter (Fungilab EVO Expert Rotational Viscometer, Global Gilson, USA) was used to measure viscosity. These measurements were based on Ay and Gunasekaran (1994). A cylinder (2 m diameter), operating at 60 rpm, captured shear stress in mPa.s every second during the process until a phase change took place, indicated by a sudden increase in the degree of viscosity, followed by progressive reduction. After this point, the matrix was gelated. Then a TA-TX2 texture analyzer (Stable Micro Systems, Surrey, UK), equipped with a 25-kg load cell, was used in a non-analysed sample. A probe with a disc ($\varnothing = 35$ mm) run at constant velocity from 1 mms to 1–50% of sample depth was employed. The texture study focused on the hardness parameter, which was represented by the maximum resistance during compression measured in g. To avoid influencing the matrix structure, samples were analysed in the above-mentioned containers at the same temperature as processing.

2.5. Statistical analysis

The physical analysis of the milk matrix during processing was studied by a one-way variance (ANOVA) study. In those cases in which the effect was significant (P-value < 0.05), means were compared by Fisher's least significant difference (LSD) procedure. The imaging analysis data were explored after applying multivariable statistical procedures to reduce dataset dimensionality. For this purpose, the multivariate unsupervised statistical method, Principal Component Analysis (PCA), was employed. The objective was to simplify the analysis of variance collected by the image data matrix obtained by continuously monitoring the curdling process. The regression studies between the curdling stage and image data were conducted by Support Vector Machines for regression (SVM-R). The aim of this procedure is to predict the milk matrix status across the process from the image data. SVM-R is an effective supervised learning methodology based on the statistical learning theory, and is often used for multivariable data analyses (Boser, Guyon, & Vapnik, 1992). The employed version was nu support vector regression (ν-SVM) and a polynomial function as the kernel. Samples were divided by stratified random sampling into a training batch (66% of data) and a testing batch (33% of data). The results were evaluated based on R^2 of prediction and error indicators: mean absolute error (MAE), mean square error (MSE) and the root mean square error (RMSE). These procedures were run with the PLS Toolbox, 6.3 (Eigenvector Research Inc., Wenatchee, Washington, USA), a toolbox extension in the Matlab 7.6 computational environment (The Mathworks, Natick, Massachusetts, USA).

3. Results and discussion

3.1. Milk curdling process

The results of the texture measurements taken during the process are shown in Fig. 2. Viscosity evolution with time is depicted in Fig. 2-A, where no differences in aggregation start times were observed, but appeared among the viscosity peaks of the different formulas. Viscosity started to change about 2 min after adding rennet. Proteolysis before that point could be active, although device sensitivity did not suffice to detect it. From that time, viscosity reached a similar slope, which indicates the same gelation velocity independently of solute concentration. That could be due to the saturation of rennet enzymes from 1% and the generation of proteolysis with no differences. Nevertheless, the maximum viscosity was different. The minimum viscosity was obtained for 1%, while 6% and 8% were the maximum values with non-significant differences between them. From these points, viscosities systematically reduced, in which case 8% slower reduction was observed compared to

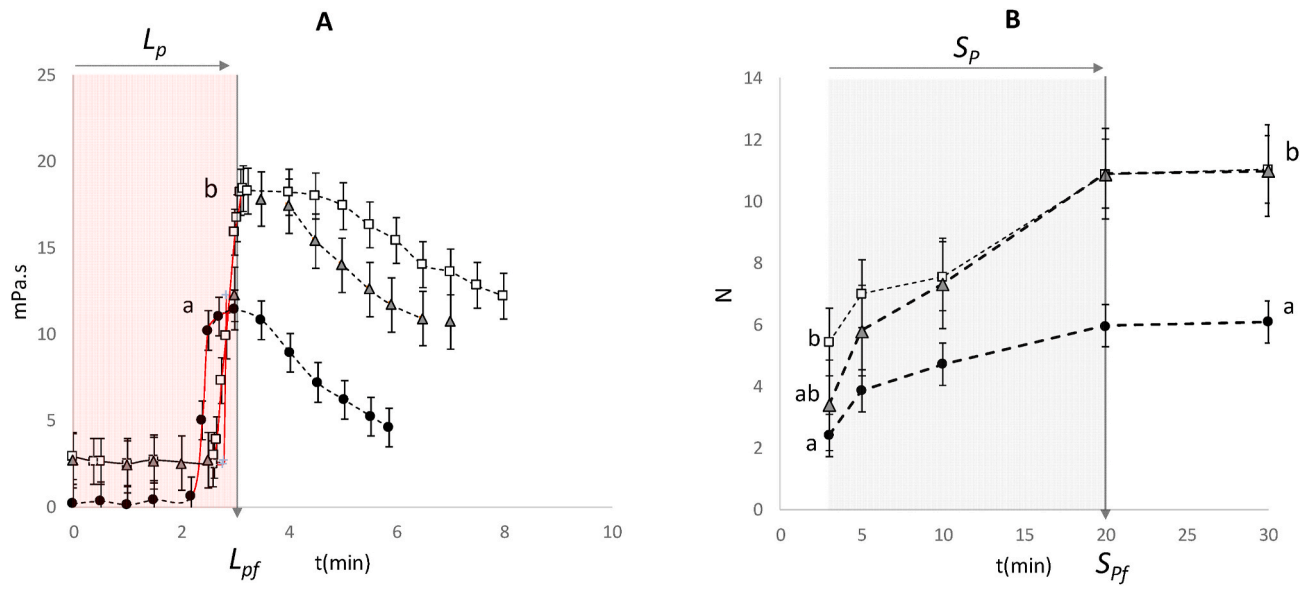

Fig. 2. The viscosity and texture analysis of the curdling process. A: viscosity evolution in the liquid phase (L_p), B: hardness evolution in the solid phase (S_p). ● 1% MP; ▲ 6% MP; □ 8% MP. L_{pf}: end of the liquid phase; S_{pf}: end of the curdling process. Watermarks indicate the phases observed for matrix physical state. Letters marks differences at $\alpha = 0.05$. Bars represent standard deviation.

6%. The observed shape of the viscosity evolutions was the typical response of the rheological measurements taken during the curdling process (Pazzola et al., 2018), where the end of the liquid phase was marked by peak viscosity from which a reduction in that property was recorded. This reduction was due to liquid leaking as a result of the gel network breaking from turning the viscosimeter cylinder (Fernández Farrés & Norton, 2014). Thus the viscosity recorded from peaks was due to the release of the liquid phase confined to the gel network, which still contained proteolytic activity and the substrate. This was evidenced by the observed results of the texture analysis done of the observed peak viscosity. The texture of the solid gels formed after 3 min, which allowed the evolution of the formed network to be observed (Fig. 2-B). Hardness was different at 3 min and increased to 20 min in all cases. However, in exactly the same way as the previously observed viscosity results, 6% and 8% did not present any differences. The observed increased hardness from the formed gel evidenced that proteolysis and aggregation phenomena overlapped (Fig. 3-A), thus the importance of differentiating between the coagulation start and end times of the curdling process.

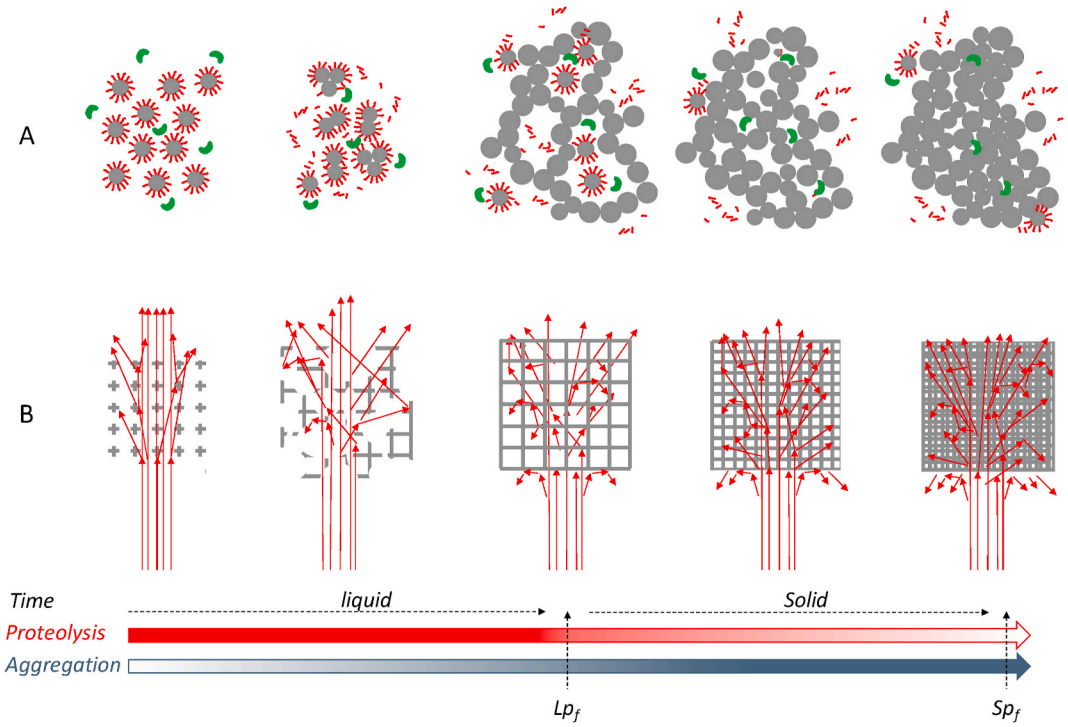

Fig. 3. Proposed scheme of casein changes and laser interaction on a microscopic scale across proteolysis and the aggregation phenomena. A: evolution of casein micelles. B: evolution of the casein network and its interaction with laser. Grey circles: casein micelles; red lines: κ-casein; green objects: enzymes; grey bars: casein network; red arrows: laser beam. (For interpretation of the references to colour in this figure legend, the reader is referred to the Web version of this article.)

The physical analysis of the process showed two defined phases: the liquid phase (L_p), where the milk matrix changed from the liquid to the solid state, and was assumed until approx. 3 min (end of liquid phase L_{pf}); the solid phase (S_p), where the formed solid matrix increased hardness because the action of the enzymes in the remaining substrate from the liquid phase were confined in the solid network and sedimentation processes, and were assumed to be between 3 and 20 min (end of solid phase evolution S_{pf}). From 20 min, the gel was assumed stable given the observed asymptotic evolution of hardness which, therefore, denoted the end of the curdling process.

3.2. Exploring image data

In this part of the study, image data were explored to know the influence of the two tested factors on the properties of the data collected by this technique. These data were collected from orthogonal images by each pixel in both intensity (grey value) and coordinates terms throughout the curdling process. Firstly, the evolution of the intensity of those pixels located in different positions was analysed. Fig. 4 shows the evolution of three pixels located in distinct zones of the captured diffraction patterns. The first was located in the middle of the saturated zone, while the other two were located at 50% and 25% of the radius length, respectively.

The kinetics of pixel intensities with time showed an initial curve and an asymptotic zone in all the formulas, although differences in curve shapes were observed. This revealed how intensity reduced due to the increasing interaction of light with casein aggregation (Fig. 3-B). These phenomena match the classic light backscattering method, followed to study this process in a laboratory, where a reduction in light transmittance was also detected in milk curdling by spectroscopic techniques (Mateo et al., 2010). Although this fact is frequently for all formulas and pixel positions, the absolute values of intensity and their evolution differed depending on coordinates and solute concentration. This revealed that the different collected data about the process depended on the coordinates of the image, which could be crucial to further study the process.

Increasing solutes also reduced laser light transmittance before diminishing the saturated zones of the captured pattern. This phenomenon meant that the properties of the image from a solid sample of 1% were better transmitted than an image from a sample of 6%, which still had a liquid matrix. It was equal between 6% and 8%. This sequence is found in Fig. 4-A, B and C.

This phenomenon has been previously observed when this imaging technique was applied to model yogurt processing from different milk species (Verdú et al., 2019b). In this case, the lowering of pH by the microorganism metabolism led to the same reduction in transmittance, and also to modifications in the diffraction patterns because of the precipitation of proteins. Likewise, differences between milks were observed mainly because of their differences in composition in both protein and lipids terms. Moreover, the effect of these changes in the milk matrix on another type of measurements has also been reported by Koc and Ozer (2008), who reported how casein aggregation lowers a product's ultrasonic attenuation coefficient.

The same study was done following the observed results by the previous three studied pixels. However in this case, the profile of the diffraction pattern was plotting with all the pixels (Fig. 5). These data were collected from the orthogonal images (Fig. 5, top right); the X-axis (blue) represents the pixel position and the Y-axis denotes time (green dotted arrow). The Z-axis in the 3D plot represents intensity (grey value).

The objective was to explore how the data collected from each zone of the diffraction patterns evolved with distinct kinetics due to both the enzyme and composition effect. Not only the time evolution of the process, but also the solute concentration can differentiate visually because of the differences in evolution in each case. This revealed that using the entire data matrix extracted from the orthogonal images would capture the specific variance from each formula with the same matrix modification. Therefore, the orthogonal images of each sample were extracted and transformed into a multivariate data matrix to study the technique's capability to model the entire process.

3.3. Modelling studies

After exploring the data collected during the curdling process by laser backscattering imaging, multivariate statistical procedures were applied to reduce the dimensionality of the imaging datasets according to the variance captured by each pixel position over time. The aim of that reduction was to study the total captured variance with only a few synthetic variables called principal components (PCs). Thus a PCA was applied to the data matrix extracted from the orthogonal images of all the formulas. The result was a reduction from 180 variables (pixel positions of intensity profile) to one PC (PC1). This PC collected 96.1% of total variance.

Fig. 6 shows how the average of the scores obtained by PC1 for each formula evolves with time, and how the variance collected by PC1 was composed of the variance produced by both the matrix evolution and solute concentration effects. However, the latter had higher variance loads, as shown by the differences in the scores at t = 0 min. The differences in raw material observed at t = 0 followed the previous differences noted in Fig. 5. The distinct solute concentrations led to modifications in the matrix-light interaction, which were captured in the images prior to enzymatic modifications. This revealed the technique's

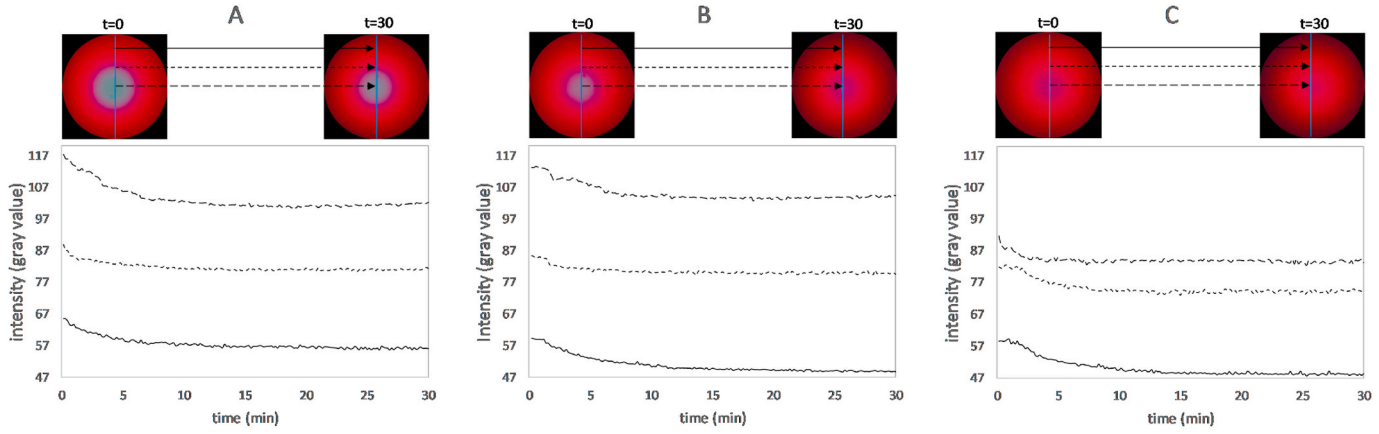

Fig. 4. Evolution of the different pixel locations from the diffraction patterns during the curdling process. A: 1% MP; B: 6% MP; C:8% MP. The blue line indicates the selected intensity profile. (For interpretation of the references to colour in this figure legend, the reader is referred to the Web version of this article.)

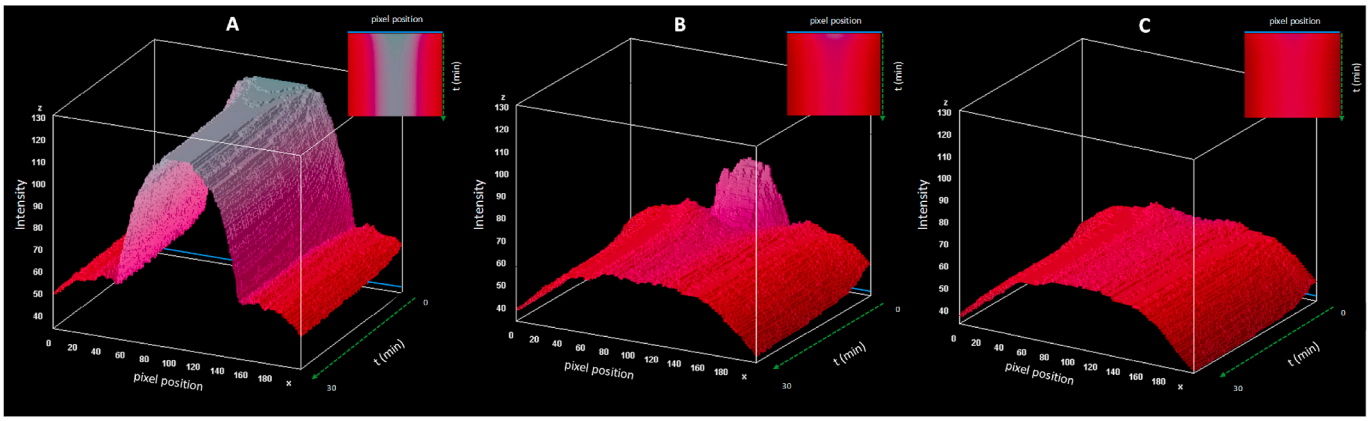

Fig. 5. Evolution of the intensity profile from diffraction patterns throughout the curdling process. A: 1% MP; B: 6% MP; C: 8% MP. The blue line indicates the selected intensity profile. The green dotted line denotes the time axis. The images in the top right zones represent the original orthogonal images. (For interpretation of the references to colour in this figure legend, the reader is referred to the Web version of this article.)

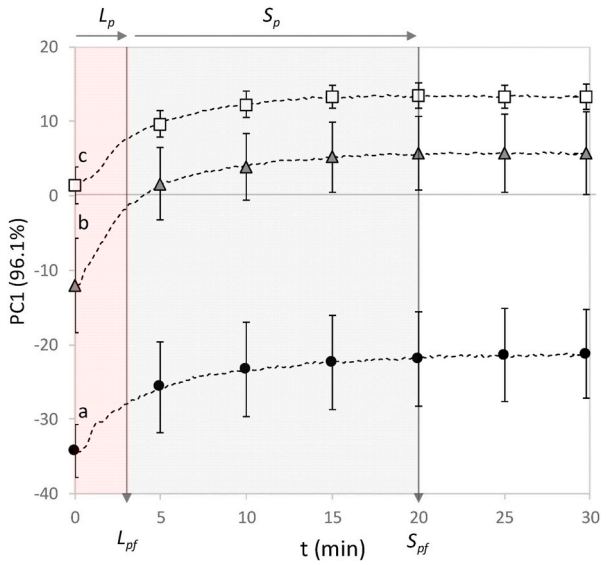

Fig. 6. Kinetics of the dimensionally reduced data from the images collected during curdling process monitoring. ● 1% MP; ▲ 6% MP; □ 8% MP. L_p: liquid phase; S_p: solid phase. L_{pf}: end of the liquid phase; S_{pf}: end of the curdling process. Watermarks indicate the phases observed for the physical matrix state. Letters mark differences at $\alpha = 0.05$. Bars represent standard deviation.

capacity to characterise the raw material composition at the beginning of processing. Unlike the data observed in the physical analysis in Fig. 2-A, the changes brought about by enzymes in the milk matrix were detected during the entire L_p, and corresponded to the start of the proteolysis phenomenon. The common behaviour involved an increase in the values from t = 0 min until asymptotic progression took place. The main difference was observed in L_p, where a more marked increase in the captured variance was observed for 6% and 8%. Fig. 6 marks the two phases observed in the physical analysis. L_p matched the zone of the maximum rise for the scores, while S_p included a moderate increase in scores to the asymptotic zone around t = 20 min.

The imaging data captured the variance generated in the matrix during the process because of both proteolysis and aggregation phenomena, which implies that the differences in the two observed phases were collected. However, no clear change in phase was observed in the space of the variance generated by this PCA. This could be due to the wide variance generated by the effect of the solute concentration on the phase change at the L_{pf} point on PC1, which was diluted.

To test this hypothesis, single PCAs were run for each formula to isolate the variance contained in the imaging data produced exclusively by matrix evolution with time, and to avoid the solute concentration effect. The results are represented in Fig. 7.

Reduction in dimensionality was common for each formula, which was done in two PCs (PC1 and PC2). These PCs accumulated more than 95% of total variance in all cases. In this case, total variance could be studied by two different PCs, which presented distinct evolutions. The results showed no differences in PCs kinetics among formulas. The plots in Fig. 7 depict the evolution of the average of PC1 and PC2 in each formula. The scores of PC1 (dotted lines) followed similar kinetics to the previous PCA simultaneously done with all the formulas (Fig. 6). However in this case, both evolutions in L_p and S_p were explained on a higher scale in score value terms. With the PCA in Fig. 5, the evolution of L_p was explained by approx. 10 score units, while the variance in this phase was explained by approx. 40 score units in single PCAs (Fig. 7). This allowed appreciating the differences between L_p and S_p, and not by a marked zone, but also with a clearer slope change. Nevertheless, PC2 evolution showed major differences compared to PC1. In this case, a main change in tendency was noted at L_{pf}, from which inverse evolution of PC1 followed until asymptotic zone S_{pf}. The differences observed in PCs in this case could be explained by the two main phenomena that took place during the process. The PC1 kinetics could be better related to proteolysis activity. This phenomenon started at t = 0 and evolved uninterruptedly with time until S_{pf} following the PC1 kinetics. However, the aggregation phenomenon overlapped proteolysis, and generated a more marked sporadic modification when the minimum casein network came about by being a solid matrix. Therefore, this event could be attributed to the variance captured by PC2. The change of phase also explained the inversion of that tendency for this PC.

Thus by avoiding the variance produced by solute concentration using single PCAs, the matrix evolution kinetics was confirmed to be equal for all formulas. This revealed that the times for the two previously observed phases in the physical analysis only minimally altered within the used solute concentration range. This agrees with the explanation of enzymes' saturation, which were worked at maximum velocity because of excess substrate in all cases.

These results suggest the possibility of modelling the curdling process of the studied formulas to predict the status of each phase per formula, or better still, for them all together. For this latter case, PC1 or PC2 of each formula (Fig. 7) was employed at the same time. So models can characterise the process by determining L_{pf} and S_{pf} from the imaging data (through PC1 or PC2, respectively). For this purpose, time was transformed into the percentage of processing (%t) to arrive at the end of each phase; that is, L_{pf} and S_{pf}, *represented* 100% of phase L_p and phase S_p, respectively. Fig. 8-A shows the combined average data of the scores obtained from each formula (Fig. 7) with the new units for time, where

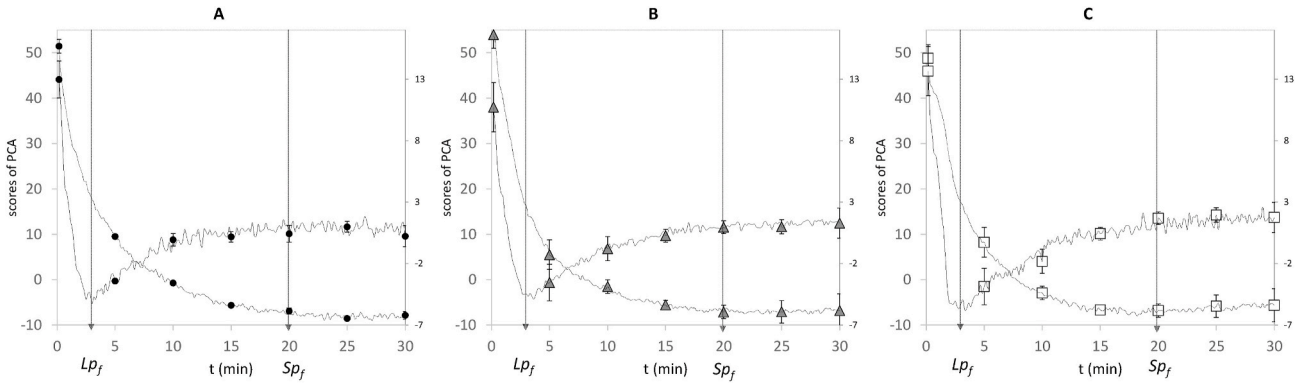

Fig. 7. Kinetics of the dimensionally reduced data from the images collected during curdling process monitoring for single solute concentrations. A = ● 1% MP; B = ▲ 6% MP; C = □ 8% MP. Dotted line: PC1; Black line: PC2. L_{pf}: end of the liquid phase; S_{pf}: end of the curdling process. Bars represent standard deviation.

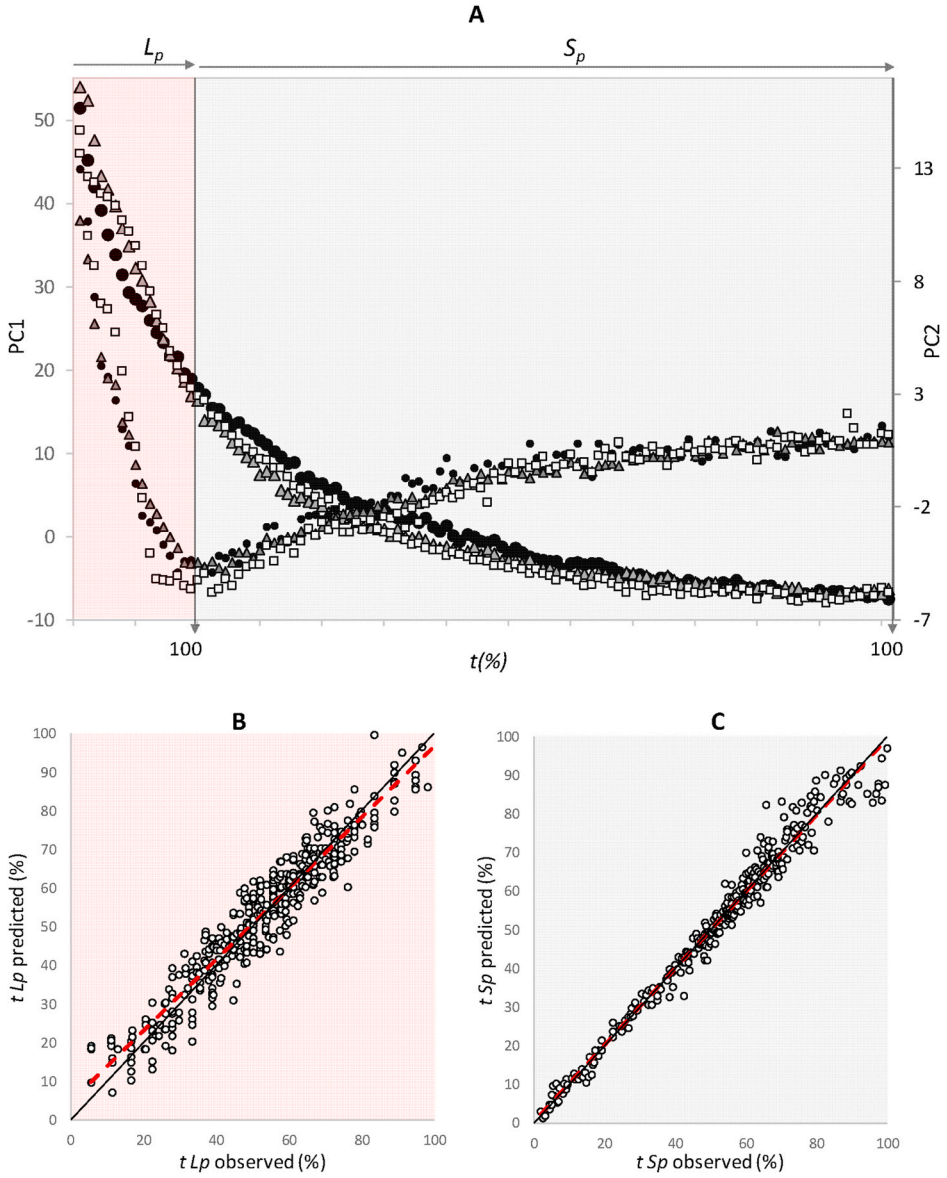

Fig. 8. Regression studies. A: The overlapping scores of PC1 and PC2 from the single studies; B and C: % t observed vs. predicted from the imaging data for L_p and S_p. ● 1% MP; ▲ 6% MP; □ 8% MP. L_p: liquid phase; S_p: solid phase.

the scores for all formulas overlap.

For modelling purposes, *SVM-R* was used for its capacity to model non-linear relations. Table 1 shows the prediction results. The obtained R^2 were higher than 0.90 for both the single and unified models, and no differences in errors were specifically observed. The modelling of %t was successfully done for both phases, although the error measurements obtained better results for S_p. This effect is observed in the differences in the dispersion of the plots of the measured vs. predicted data included in Fig. 8-A and 8-B. These plots correspond to the unified model. These differences are explained by the milk matrix properties during L_p. This can generate wider variability in diffraction patterns because of the movements of the own dispersed components and formed protein flocs across the still fluidised matrix. This effect can be reduced at L_{pf}, when the matrix change to the solid status occurs to then generate stable interactions with laser-light despite proteolysis and aggregation continuing until S_{pf}.

The results report that the data captured and extracted from laser backscattering imaging strongly depended on the milk changes produced by both proteolysis and aggregation, which means that it can be used to predict the matrix status during the curdling process. This prediction can be done independently of solute concentration and within the range studied in this experiment. Note that although this experiment shows the capacity of this technique on the laboratory scale, the observed phenomenon can be adapted to an industrial scale by making several modifications to the device. Some of these modifications would focus on features such as laser power, the placement and properties of the capture system, etc., to collect information about light-matrix interaction during the real industrial process, but adapted to velocity, the environment and the containers made with different materials.

4. Conclusions

Laser backscattering imaging's capacity to characterise and model milk curdling phase kinetics in a non-destructive mode was evidenced for the formulas tested in this experiment. The diffraction patterns generated because of the milk matrix and laser interaction depended on both solute concentration and curdling process status. This means that these dependencies offer the possibility of capturing the variance generated by both composition features and enzyme activity. These features allowed the changes in the physical matrix states to be continuously monitored and to, therefore, determine the limits of both curdling process phases. Transmittance reduced with both increased solute concentration and gel formation. Moreover, the kinetics of both proteolysis and aggregation phenomena were modelled after eliminating the effect of solute concentration. The change in phase, due to the formation of the minimum solid gel network and its evolution, can be modelled by imaging data, which generated accurate regression models for each phase. These models gave accurate predictions for both single and unified approaches. Therefore, it was concluded that the laser backscattering imaging technique presents suitable properties to be used as a non-destructive tool for continuous curdling process monitoring during the cheese-making process. New studies are being done to know the influence of factors, such as origin of milk, fat fraction and different temperatures, on the technique's observed skills.

CRediT authorship contribution statement

Samuel Verdú: Conceptualization, Methodology, Formal analysis, Investigation, Writing - original draft, Supervision, Visualization. **Alberto J. Pérez:** Software, Data curation, Writing - original draft. **José M. Barat:** Project administration, Funding acquisition, Supervision. **Raúl Grau:** Conceptualization, Writing - review & editing, Supervision, Project administration, Funding acquisition, Resources.

Table 1
Prediction parameters for the regression models between curdling status and imaging data.

Formula	*Phase*	*Model parameters*			
		MSE	*RMSE*	*MAE*	R^2
1%	L_p	73.54	8.114	6.046	0.931
	S_p	17.887	4.229	3.352	0.967
6%	L_p	69.146	8.315	6.615	0.933
	S_p	14.523	3.811	2.443	0.973
8%	L_p	73.012	8.545	6.598	0.927
	S_p	44.514	6.672	4.882	0.937
Unified model	L_p	68.7	8.3	6.6	0.92
	S_p	28.7	5.4	3.9	0.95

L_p: liquid phase; S_p: solid phase. R^2: Correlation coefficient observed vs. predicted; MAE: mean absolute error; MSE: mean square error: RMSE: root mean square error.

Declaration of competing interest

The authors declare that they have no known competing financial interests or personal relationships that could have appeared to influence the work reported in this paper.

Acknowledgment

The authors gratefully acknowledge the financial support from the University Polytechnic of Valencia for Programme "Ayudas para la Contratación de Doctores para el Acceso al Sistema Español de Ciencia, Tecnología e Innovación, en Estructuras de Investigación de la UPV (PAID-10-17)".

References

Aldalur, A., Ong, L., Bustamante, M.Á., Gras, S. L., & Barron, L. J. R. (2019). Impact of processing conditions on microstructure, texture and chemical properties of model cheese from sheep milk. *Food and Bioproducts Processing*. https://doi.org/10.1016/j.fbp.2019.05.003.

Arango, O., & Castillo, M. (2018). A method for the inline measurement of milk gel firmness using an optical sensor. *Journal of Dairy Science*. https://doi.org/10.3168/jds.2017-13595.

Ay, C., & Gunasekaran, S. (1994). *Ultrasonic attenuation measurements for estimating milk coagulation time*. Transactions of the American Society of Agricultural Engineers. https://doi.org/10.13031/2013.28151.

Bittante, G., Penasa, M., & Cecchinato, A. (2012). Invited review: Genetics and modeling of milk coagulation properties. *Journal of Dairy Science, 95*(12), 6843–6870. https://doi.org/10.3168/jds.2012-5507.

Boser, B. E., Guyon, I. M., & Vapnik, V. N. (1992). A training algorithm for optimal margin classifiers. *Proceedings of the 5th Annual ACM Workshop on Computational Learning Theory*, 144–152. https://doi.org/10.1145/130385.130401.

Castillo, M., González, R., Payne, F. A., Laencina, J., & López, M. B. (2005). Optical monitoring of milk coagulation and inline cutting time prediction in Murcian al Vino cheese. *Applied Engineering in Agriculture*.

Curti, E., Pardu, A., Del Vigo, S., Sanna, R., & Anedda, R. (2019). A low-field Nuclear Magnetic Resonance dataset of whole milk during coagulation and syneresis. *Data in Brief*. https://doi.org/10.1016/j.dib.2019.104520.

Darnay, L., Králik, F., Oros, G., Koncz, Á., & Firtha, F. (2017). Monitoring the effect of transglutaminase in semi-hard cheese during ripening by hyperspectral imaging. *Journal of Food Engineering*. https://doi.org/10.1016/j.jfoodeng.2016.10.020.

Everard, C. D., O'Callaghan, D. J., Fagan, C. C., O'Donnell, C. P., Castillo, M., & Payne, F. A. (2007). Computer vision and color measurement techniques for inline monitoring of cheese curd syneresis. *Journal of Dairy Science*. https://doi.org/10.3168/jds.2006-872.

Fernández Farrés, I., & Norton, I. T. (2014). Formation kinetics and rheology of alginate fluid gels produced by in-situ calcium release. *Food Hydrocolloids, 40*, 76–84. https://doi.org/10.1016/j.foodhyd.2014.02.005.

Harton, K., & Shimizu, S. (2019). Statistical thermodynamics of casein aggregation: Effects of salts and water. *Biophysical Chemistry, 247*, 34–42. https://doi.org/10.1016/j.bpc.2019.02.004. February.

Jiménez, A., Rufo, M., Paniagua, J. M., Crespo, A. T., Guerrero, M. P., & Riballo, M. J. (2017). Contributions to ultrasound monitoring of the process of milk curdling. *Ultrasonics*. https://doi.org/10.1016/j.ultras.2017.01.007.

Koc, A. B., & Ozer, B. (2008). Nondestructive monitoring of renetted whole milk during cheese manufacturing. *Food Research International, 41*(7), 745–750. https://doi.org/10.1016/j.foodres.2008.05.008.

Lomholt, S. B., Worning, P., Øgendal, L., Qvist, K. B., Hyslop, D. B., & Bauer, R. (1998). Kinetics of the renneting reaction followed by measurement of turbidity as a function of wavelength. *Journal of Dairy Research*. https://doi.org/10.1017/S0022029998003148.

Mateo, M. J., O'Callaghan, D. J., Everard, C. D., Castillo, M., Payne, F. A., & O'Donnell, C. P. (2010). Evaluation of on-line optical sensing techniques for monitoring curd moisture content and solids in whey during syneresis. *Food Research International*. https://doi.org/10.1016/j.foodres.2009.09.023.

O'Callaghan, D. J., O'Donnell, C. P., & Payne, F. A. (2002). Review of systems for monitoring curd setting during cheesemaking. *International Journal of Dairy Technology*. https://doi.org/10.1046/j.1471-0307.2002.00043.x.

Panthi, R. R., Kelly, A. L., Sheehan, J. J., Bulbul, K., Vollmer, A. H., & McMahon, D. J. (2019). Influence of protein concentration and coagulation temperature on rennet-induced gelation characteristics and curd microstructure. *Journal of Dairy Science, 102*(1), 177–189. https://doi.org/10.3168/jds.2018-15039.

Pazzola, M., Stocco, G., Paschino, P., Dettori, M. L., Cipolat-Gotet, C., Bittante, G., & Vacca, G. M. (2018). Modeling of coagulation, curd firming, and syneresis of goat milk from 6 breeds. *Journal of Dairy Science, 101*(8), 7027–7039. https://doi.org/10.3168/jds.2018-14397.

Vacca, G. M., Stocco, G., Dettori, M. L., Bittante, G., & Pazzola, M. (2020). Goat cheese yield and recovery of fat, protein, and total solids in curd are affected by milk coagulation properties. *Journal of Dairy Science*. https://doi.org/10.3168/jds.2019-16424.

Verdú, S., Barat, J. M., & Grau, R. (2019a). Laser backscattering imaging as a non-destructive quality control technique for solid food matrices: Modelling the fibre enrichment effects on the physico-chemical and sensory properties of biscuits. *Food Control*. https://doi.org/10.1016/j.foodcont.2019.02.004.

Verdú, S., Barat, J. M., & Grau, R. (2019b). Non destructive monitoring of the yoghurt fermentation phase by an image analysis of laser-diffraction patterns: Characterization of cow's, goat's and sheep's milk. *Food Chemistry, 274*, 46–54. https://doi.org/10.1016/j.foodchem.2018.08.091. July 2018.

Verdú, S., Pérez, A. J., Barat, J. M., & Grau, R. (2018). Laser backscattering imaging as a control technique for fluid foods: Application to vegetable-based creams processing. *Journal of Food Engineering, 241*, 58–66. https://doi.org/10.1016/j.jfoodeng.2018.08.003. May 2018.

Verdú, S., Ruiz-Rico, M., Pérez, A. J., Barat, J. M., & Grau, R. (2020). Application of laser backscattering imaging for the physico-chemical characterisation of antimicrobial silica particles functionalised with plant essential oils. *Journal of Food Engineering*. https://doi.org/10.1016/j.jfoodeng.2020.109990.